International Conference on Advanced Optical Diagnostics
in Fluids, Solids and Combustion
December 4-6, 2004, Tokyo, Japan
V0020

Aero-Optical Measurements Using Malley Probe and High-Bandwidth 2-D Wavefront Sensors.

Gordeyev S.*[1], Duffin D.*[2] and Jumper E.*[3]

*1 Dept. of Aerospace and Mechanical Engineering, University of Notre Dame,
Notre Dame, IN, 46556, USA
Tel:+1-574-631-4338 / FAX:+1-574-631-8355
E-mail: sgordeye@nd.edu
*2 Dept. of Aerospace and Mech. Eng., University of Notre Dame, Notre Dame, IN, 46556, USA
*3 Dept. of Aerospace and Mech. Eng., University of Notre Dame, Notre Dame, IN, 46556, USA

Abstract: Two analog high-bandwidth wavefront devices to obtain temporally resolved wavefronts are presented. The first device is called a Malley probe which provides one-dimensional slices of optical wavefronts in the streamwise direction; the second device is a high-bandwidth two-dimensional wavefront sensor capable of sampling wavefronts on a continuous basis with sampling rates up to 125 kHz. These devices were compared against a commercially-available, two-dimensional wavefront sensor for laser propagation through an acoustically forced planar heated jet. The comparison demonstrated that the two high-temporal-bandwidth wavefront sensors provided essentially the same information about the aberrating flow structure. Feasibility of significantly reducing optical aberrations using feed-forward adaptive optics is discussed.

Keywords: Aero-Optics, Optical Path Difference, OPD, wavefront measurements

1. Introduction

When a collimated laser beam travels through a medium with a variable index of refraction, its wavefront gets distorted. When the transmission distance through the medium is relatively small and the aberrations are caused by a flow with a changing density field, these effects are called *aero-optical effects*, (Gilbert and Otten, 1982). High-speed compressible turbulent flows around an aircraft change the local index-of-refraction and impose fast-changing optical aberrations on an airborne laser beam's wavefronts. These aberrations degrade the laser beam's ability to be focused in the far-field, thus reducing its intensity on a target. The reduction in the intensity on target causes a reduction in system performance for communication, interrogation and targeting or a directed-energy weapon system (Jumper and Fitzgerald, 2001).

Until relatively recently the full impact of aero-optical effects on airborne direct energy laser weapon systems was not understood. Only in recent years actual optical measurements of the aberrating environment imposed by separated flows over the exit pupils of the beam directors have been shown to greatly limit the lethal field of regard of the weapons systems. Measurements made at the Arnold Engineering and Development Center (AEDC) and at the University of Notre Dame for flight Mach-number conditions from 0.7 – 0.8 showed the aberrating environment posed by separated flows through which lasers are projected could reduce the lasers' lethality to 1% of its

otherwise diffraction-limited performance (Cicchiello and Jumper, 1997).

The fast evolving convecting turbulent structures which are present in turbulent flows and responsible for the aberrations usually exhibit high spatial and temporal bandwidths. Therefore, premier among the instruments' characteristics to acquire optical wavefronts is their ability to capture long time series of time-resolved, high-bandwidth, two-dimensional wavefronts. In order to resolve the important aberrations, temporal bandwidths must exceed 50 kHz. Most commercially available 2-D wavefront sensors rely on a digital CCD camera and, although usually providing an excellent spatial resolution, sampling rates are typically limited to a few hundred frames per second. These rates are far lower then desired sampling frequencies to correctly resolve optical aberrations, which are on the order of tens of kilohertz. Furthermore, in a wind-tunnel testing environment aberrations caused by aero-optic flows of interest must be separated from other wavefront aberrations that are necessarily superimposed on the wavefronts due to the testing environment, such as tunnel/floor vibrations, temperature variations in the main tunnel flow and flow over insertion and extraction windows, to name a few.

We have developed two relatively inexpensive complimentary analog devices to measure optical aberrations at high sampling rates. The first device is called a Malley Probe sensor and provides highly resolved one-dimensional slices of Optical Path Difference (OPD) in the streamwise direction. It measures jitter signals on two closely spaced parallel baser beams and, by correlating the signals using a spectral method, provides temporal OPD evolution at the measurement station with sampling rates up to 200 kHz. Utilizing the spectral method also allows one to filter out any unphysical vibration-related contamination, usually imposed on laser beams in a typical experimental environment. In addition, the sensor gives valuable information about average convective speeds of optically-active structures that may also have different scale sizes.

The second device is a high-speed analog Shack-Hartmann sensor. It utilizes an array of analog position sensing devices, and the sampling rates up to 125 kHz are possible, with limited, but useful spatial resolution. It provides continuous long time-series of the wavefronts' evolution and a similar procedure for removing vibrations used in the Malley probe can be applied.

A test experiment using a slightly-heated low-speed planar jet was conducted to verify the validity and accuracy of optical wavefront measurements using both these devices. A low-speed commercially available 2-D wavefront sensor was used to make benchmark measurements. Streamwise evolution of roll-up structures and its convective nature were correctly captured in the wavefronts using both the Malley probe and the high-speed wavefront sensor.

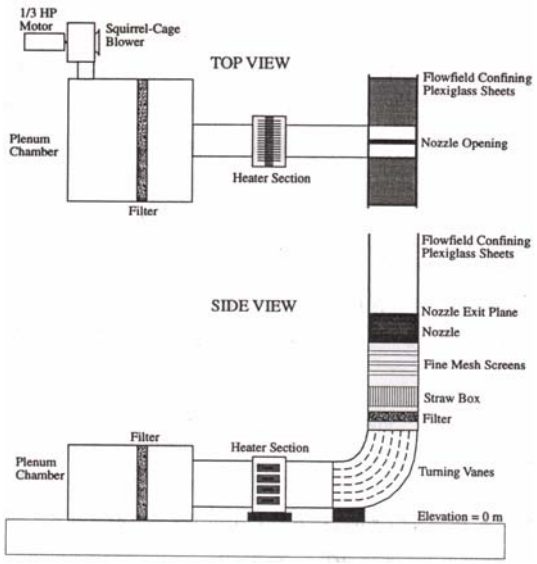

Figure 1. Two-dimensional heated jet facility (Hugo, 1995).

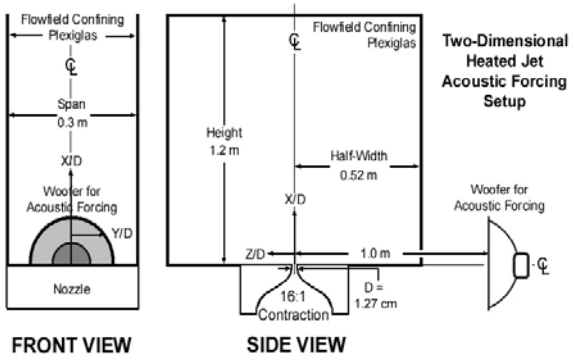

Figure 2. Heated jet exit plane schematic.

2. Heated Jet Facility

2.1 Facility Description.

The heated-jet facility is shown schematically in Fig. 1. It consists of a plenum chamber pressurized above atmospheric pressure by a squirrel-cage-type blower. After passing through filters and a slight contraction, air enters a rectangular duct with a series of heaters located approximately 1 m from its entrance and 1 m from a ninety degree finned bend so that the heated air is now moving vertically in a rectangular duct with filters and flow straighteners as shown in Fig. 1. The flow then passes through a 16-to-1 two-dimensional nozzle to an exit nozzle width, *D*, of 12.7 mm. The heated jet leaves the nozzle with a core velocity of 7 m/s. The detailed fluid mechanic measurements for this jet can be found in Hugo (1995).

Figure 2 shows a schematic of the exit plane of the nozzle and an associated system of coordinates. The left side of the figure shows a view normal to the span of the jet (the aero-optic view) showing the span dimension, 30 cm, and the end plates aligned in the flow direction to help reduce three-dimensional effects that would otherwise be present if the jet were to be uncontained. The right side of the figure shows a view along the cross-stream direction of the jet showing a number of important details. First, the jet exit plane forms a solid floor that extends for 0.52 m in each direction from the nozzle gap. Second, the location and orientation of a speaker used to force the flow is shown; this speaker is located in the exit plane 1 m from the center line of the nozzle.

2.2 Jet's Response to Acoustical Forcing.

The details of the jet's response to acoustic forcing can be found in Duffin et. al. (2004). It is sufficient here to briefly describe the jet's characteristics used for the comparisons reported here. The acoustic forcing was provided by a Pyramid PWFX107 600W 10" woofer located as shown in Fig. 2. The speaker was driven by a Crown CE2000 PA amplifier with an input provided by an Agilent Model 33120A function/arbitrary waveform generator. In the present case the jet was forced with a 240 Hz sine waveform.

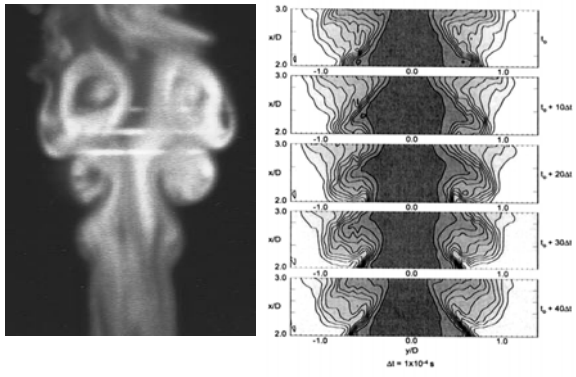

Figure 3. Smoke visualization of the two-dimensional heated jet (left), and phase-averaged temperature profiles of the jet (right) (Hugo and Jumper, 1995a).

The jet's response to the 240 Hz forcing was to regularize the jet's most-unstable Kelvin-Helmholtz instability in the jet's two free shear layers. Depending on the amplitude of the acoustic signal, the first roll-up can be adjusted closer or further away from the nozzle exit plane. The forcing also regularizes the first pairing resulting in the formation of 120 Hz sub-harmonic, larger-coherence-length flow structures; however, this regularization is slightly less robust than the first roll-up. In order to provide the best 120 Hz regularization the amplitude of the acoustic signal caused the 240 Hz roll-up to occur somewhat closer to the exit plane than used and reported in earlier studies, which concentrated primarily on the 240 Hz structures (Hugo and Jumper, 1995a; Hugo and Jumper, 1996). In these earlier studies, the two-dimensional heated jet facility was acoustically forced in a manner similar to this present experiment. A smoke visualization of the jet and the phase-locked-averaged temperature field collected for the forced jet is shown in Fig. 3. Figures 4 and 5 show the effect that the acoustic forcing had on the jet's *OPD* pattern. Figure 4 is the heated jet's *OPD* pattern without acoustic forcing. One should note that the *OPD* peaks are quite random and while there is a certain temporal frequency to this pattern, there is also a large standard deviation about this frequency. Figure 5 shows that acoustic forcing regularizes both the amplitude of the *OPD* as well as the temporal frequency of the pattern. It is this predictable, repeatable *OPD* pattern that was used to inter-calibrate the wavefront measurement devices for this study.

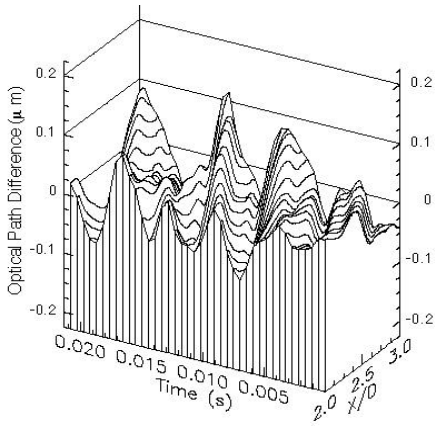

Figure 4. Time series of experimentally-measured *OPD*'s from propagation through a two-dimensional heated jet without acoustic forcing (Hugo and Jumper, 1996)

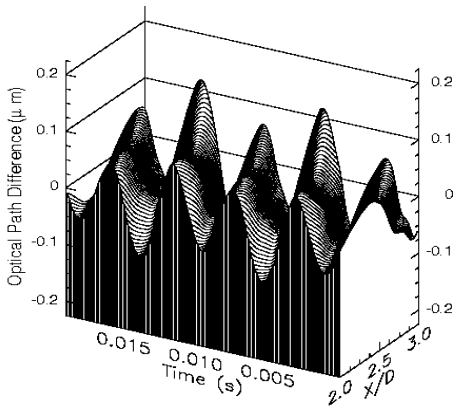

Figure 5. Time series of experimentally-measured *OPD*'s from propagation through a two-dimensional heated jet with acoustic forcing (Hugo and Jumper, 1995b)

3. Wavefront Sensors.

3.1 Malley Probe

The Malley Probe is an optical instrument that can make direct, accurate measurements of dynamically-distorting wavefronts, including the character of the *OPL(t)*. This is done by projecting small-aperture (~1mm) laser beams through the aberrating flow and measuring deflection or jitter angles θ(t) of the beams. According to Huygens's Principle, these beams will emerge from the aberrating flow normal to the wavefront of a larger-aperture laser beam projected through the same flow field. Thus, the deflection angle of the small aperture beam is just the negative spatial gradient of the Optical Path Length, *OPL*, at the probe-beam location, $\theta(x,y,t) = -\text{grad } OPL(x,y,t)$. The instantaneous deflection angle measurement procedure is presented schematically in Figure 6. A small aperture laser beam passes through a turbulent flow of interest and gets deflected. The laser beam is then focused on a Position Sensing Device (sometimes called Lateral Displacement Sensor), which accurately measures the beam's centroid position Δ(t) as a function of time. The deflection angle is calculated as $\theta(t) = \Delta(t)/f$, where f is the lens focal distance. Since the position sensing device is an analog photosensitive crystal with an almost zero response time constant, it allows sampling deflection angles at high sampling rates, on the order of hundreds of kilohertz.

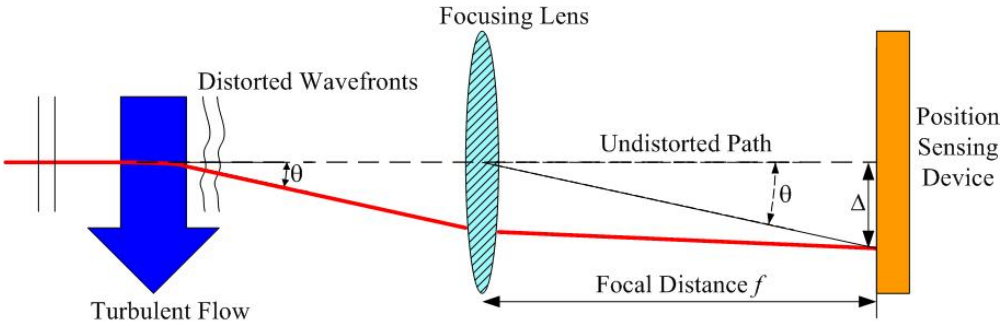

Figure 6. Principle of deflection angle measurements.

The instrument itself is a further development by Notre Dame of an instrument described in a paper by Malley, et. al. (1992). The Notre Dame instrument consists of two closely spaced small-aperture beams (beam diameter ~ 1 mm spaced 2-5 mm apart and aligned in the streamwise direction); the second beam is used to extract phase or convection velocity of the optically aberrating structure, U_c, by cross-correlating the two signals and obtaining the time delay for maximum correlation. Knowing the distance between the two beams and the delay time, the convection velocity of the optical aberrations can be computed. A more-robust method of

determining the convection velocity using a spectral method is described in Gordeyev et. al. (2003). As described in Hugo and Jumper (1995c) and Hugo and Jumper (1996), the deflection angle of the probe beam is the spatial derivative of the wavefront. The convection velocity is then needed to unfold the *OPL* using the fact that the aberrations "convect" with the fluid structures,

$$OPL(x,t) = \int_{t_o}^{t} \left(\frac{d\,OPL}{dx} \right)_{x_o} \left(\frac{dx}{dt} \right) dt = \int_{t_o}^{t} [-\theta(t)] U_c \, dt. \tag{1}$$

Once $OPL(x_o, t)$ is known at the single probe location, x_o, a Taylor's frozen flow hypothesis can be made to project *OPL* upstream and downstream by trading time and position as,

$$OPL(x_i, t) = OPL(x_o \mp U_c \Delta\tau_i, t), \tag{2}$$

where

$$\Delta\tau_i = \frac{|x_i - x_o|}{U_c}, \tag{3}$$

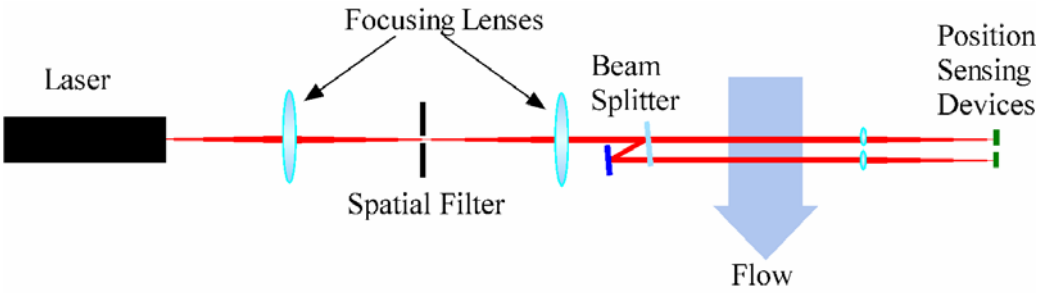

Figure 7. Schematic of a Malley Probe layout.

where in Eq. (2) the "-" is for upstream construction and the "+" is for downstream construction (i.e., upstream wavefront information has not arrived at the probe location by time t). Once the extrapolated *OPL* is known for all locations, up and downstream from the measurement location an aperture size, A, may be constructed centered on the probe location and extending up and downstream from that location a distance $A/2$. Clearly, the larger A is chosen, the less accurate the wavefront reconstruction; however, Hugo and Jumper (1995c) have shown that even though the actual wavefronts are inaccurate, all of the relevant optical information can be extracted from the extrapolated wavefront over a surprisingly large aperture. Once $OPL(x,t)$ has been extrapolated over the aperture the mean *OPL* over the aperture at each instant in time can be removed, frame-by-frame, to give $OPD(x, t)$.

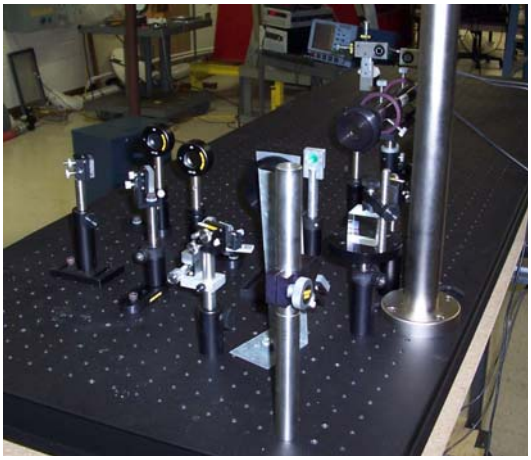

Figure 8. Optical bench layout of a Malley Probe.

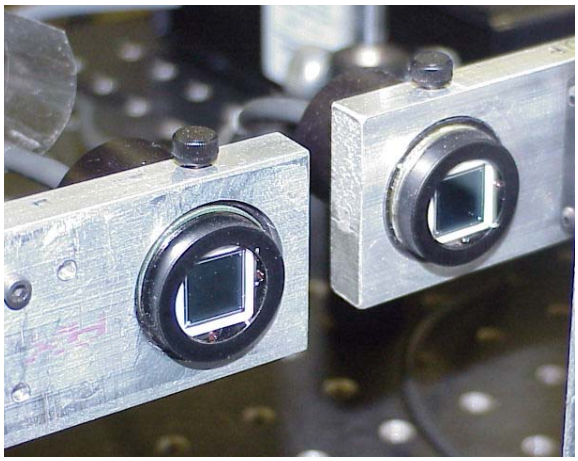

Figure 9. Position sensing devices.

Malley Probe data are also meaningful in a heavy vibration environment because the raw data are in the form of a time series of wavefront slope data (jitter data). The spectral method for extracting the convection velocity referred earlier (Gordeyev et. al., 2003) also provides information about the band of frequencies (usually less than 500 Hz) where the jitter on the two beams is not convecting but stationary; such non-convecting jitter signals infer that they are caused by vibration. Knowing the bandwidth where the vibrations reside means that these can be filtered out of the data using a high-pass filter or other more-specialized removal methods. Usually the aero-optic data is higher than the vibration filter cut-off frequency, so that no meaningful aero-optical information is lost.

A simplified schematic of the optical arrangement of a Malley Probe is shown in Fig. 7 and a typical Malley Probe set-up is shown in Fig. 8, which shows a He-Ne laser, a pin-hole and focusing optics, a beam splitter that splits the beam into two closely-spaced beams, beam-steering optics to take the beams to and return them from the region of interest, focusing lenses and finally position sensing devices placed at the focal plane of the two focusing lenses. The position sensing devices are shown in Fig. 9.

3.2 Commercially Available Wavefront Sciences Wavefront Sensor

Before discussing the high-bandwidth wavefront sensor, a typical commercially available wavefront sensor, such as the Wavefront Sciences CLAS-2D wavefront sensor will be described. This wavefront sensor is a traditional Shack-Hartmann sensor (Geary, 1995); the principle of operation is shown in Figure 10. The incoming wavefront is intercepted by a lenslet array and an average wavefront slope over each lens sub-aperture is measured by measuring dot displacements at the focal plane, similar to of Malley probe principle presented in Figure 6. Knowing slopes at finite points the wavefront is reconstructed using a Southwell method, for instance (Southwell, 1980). The displacement sensor head itself is a CCD camera (without a lens) with, in the present case, a 33 x 44 lenslet array permanently aligned and mounted over the CCD array at the lenslet focal distance. The camera is framed by an off-the-shelf frame grabber, which in the present case can be single-frame externally triggered, or can be run at a framing rate of 30 Hz. Clearly, the framing rate is insufficient to time resolve aero-optical flows of any practical importance; however, in the present case, with the heated jet acoustically forced as described in an earlier section, a pseudo-time-resolved time series of phase-locked-averaged wavefronts can be collected for the purpose of comparison with time-resolved wavefront-measuring instruments. Otherwise, when used in conjunction Malley Probe sensor, many time-uncorrelated wavefronts can be collected along with the time-resolved data to serve as a database for inferring the spanwise correlations used to construct far-field patterns.

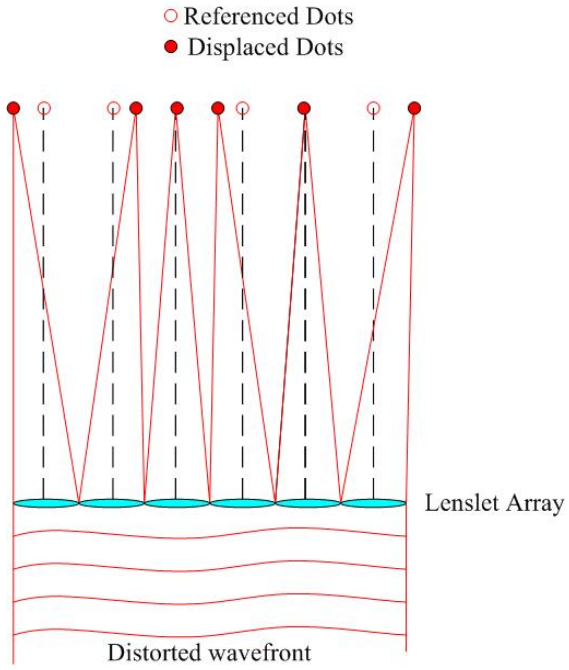

Figure 10. Shack-Hartmann sensor: principle of operation.

It is important to note that both piston and tilt must also be removed from the two-dimensional wavefronts. Further, when used as a "sanity check" for interpretation of the Malley-Probe data, a streamwise one-dimensional cut through the wavefront must first be made and its mean and tilt removed. It is important to note that non-time-resolved wavefronts contain no frequency information, and vibration contamination

can only be removed by assuming that the average tilt over the aperture is due solely to vibration.

3.3 High-Bandwidth Wavefront Sensor

Commercially available wavefront sensors use a CCD array to determine dots' positions. CCD sensors satisfy and exceed the spatial requirements for a wavefront sensor to perform testing for aero-optics; however, no sensor can even approach the temporal bandwidth needed to properly study aero-optics effects as laid out in the previous sections. Typical so-called high-speed wavefront sensors are bandwidth limited to approximately 1 kHz, an almost two-order-of-magnitude shortfall on the bandwidth requirements detailed above.

Figure 10. Notre Dame high-bandwidth wavefront sensor: overall view with a box cover removed.

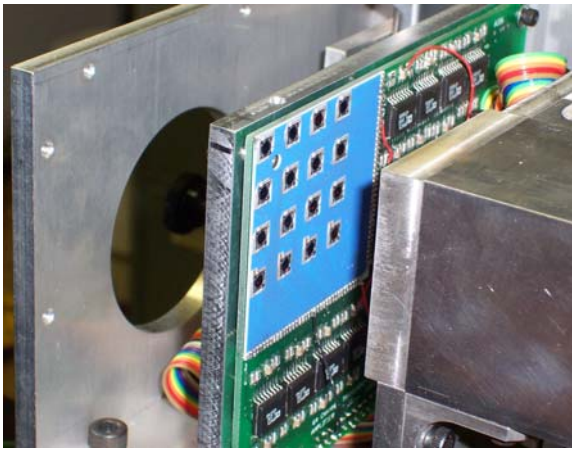

Figure 11. Notre Dame high-bandwidth wavefront sensor: a board with position sensing devices.

In order to address the temporal bandwidth shortfalls of CCD-based sensors, Notre Dame had developed a Shack-Hartmann sensor using an array of analog position sensing devices to capture focal plane dot displacements. Replacing the CCD array with an array of analog position sensing devices that have response rates in excess of 200 ns allows for a dramatic increase in temporal sampling rates up to hundreds of kilohertz, although it comes with a price of reducing spatial resolution. The overall view of the Notre Dame high-speed wavefront sensor is given in Figure 10 with a close-up of the PSD array presented in Figure 11. The wavefront sensor uses a 4 X 4 lenslet array 40 mm X 40 mm of total aperture with a board of 16 PSDs to capture mean wavefront slopes over 16 sub-apertures. For this 4 X 4 lenslet array a capture rate of 125 kHz has been demonstrated. The wavefront units are designed in such a way they can be ganged together to achieve 4 X 8 and 8 X 8 lenslet sub-apertures.

4. Heated jet wavefront results.

4.1 Baseline Flow.

The heated jet facility at Notre Dame was used as a benchmark flow to characterize different wavefront sensors in Duffin et. al. (2004), so the interested reader is referred to this paper for an extensive discussion about the flow quality and a complete description of the flow structure. Here we will highlight only the essential features of the flow. The flow is acoustically forced at 240 Hz with a speaker to expedite and stabilize the development of the vortical structure, as seen in Figure 3. The first roll-up occurs at x/D = 1 with a subsequent structure pairing occurring approximately at x/D = 2.0..2.5, where D = 12.7 mm is the jet width. To acquire wavefronts in the streamwise direction for a range of x/D = 0.5..2.5, a He-Ne collimated laser beam of 25 mm diameter was propagated through the jet normal to the jet's plane (*t.e.* along the z-direction) and directed onto the optical bench using beam-steering mirrors. The CLAS-2D wavefront sensor was used to capture series of phase-locked wavefronts using 240 Hz forcing frequency as a locking frequency.

The results in Figure 12 show typical instantaneous realizations of two-dimensional wavefronts collected with the Wavefront Sciences sensor. When the jet is acoustically locked, as in these experiments, the presumption is that the jet becomes two-dimensional, that is to say the flow structure in the x-direction is repeated at all span, y, locations. The two-dimensional wavefronts in Figure 12 indicate that this presumption, although not perfect, is closely approximated by the flow. Further, the convective nature of the aberration through the aperture is clearly apparent in the realizations. Roll-up of the first aberrating structure can be seen to clearly developed after x/D = 1 with the wavefront amplitude being around 0.1 microns.

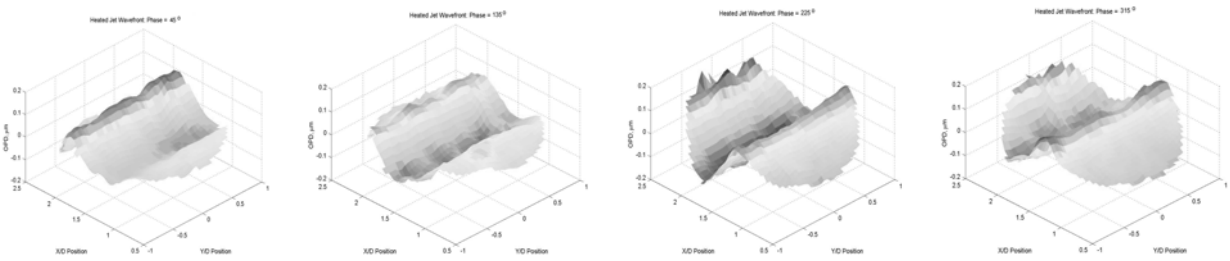

Phase = 45° **Phase = 135°** **Phase = 225°** **Phase = 315°**

Figure 12. Typical instantaneous wavefronts obtained with the Wavefront Sciences CLAS-2D wavefront sensor at various phase angles (-1.0 < Y/D < 1.0; 0.5 < X/D <2.5; OPD scale in μm).

4.2 Malley probe set-up and data reduction procedure.

For the Malley Probe, the first probe beam was placed at $X/D = 1.5$, the second Malley Probe beam was placed $\delta/D = 0.25$ downstream from the first probe beam. Time series of data were taken at a sampling rate of 100 kHz and these data were used to extrapolate wavefronts up and downstream to an overall aperture of $X/D = 0.5$ to 2.5 by presuming that the frozen-flow hypothesis is strictly true, as described in Eqs. (1)-(2). The piston and tilt modes were removed from each wavefront "frame".

4.3 Comparison of wavefront sensors.

A sampling rate of 125 kHz was used to acquire wavefronts using the high-bandwidth wavefront sensor, but only each 20th frame was used to represent the data, providing wavefronts at ~ 6 kHz. Data were phase-locked with the 240 Hz forcing frequency and averaged over 100 ensembles to get phase-averaged wavefronts. Results for selected phases are presented in Figure 13 and the link to the full Movie 1 is given at the end of the paper. A comparison with highly spatially resolved phase-locked wavefronts using the CLAS-2D wavefront sensor, Figure 12, revealed that, although the

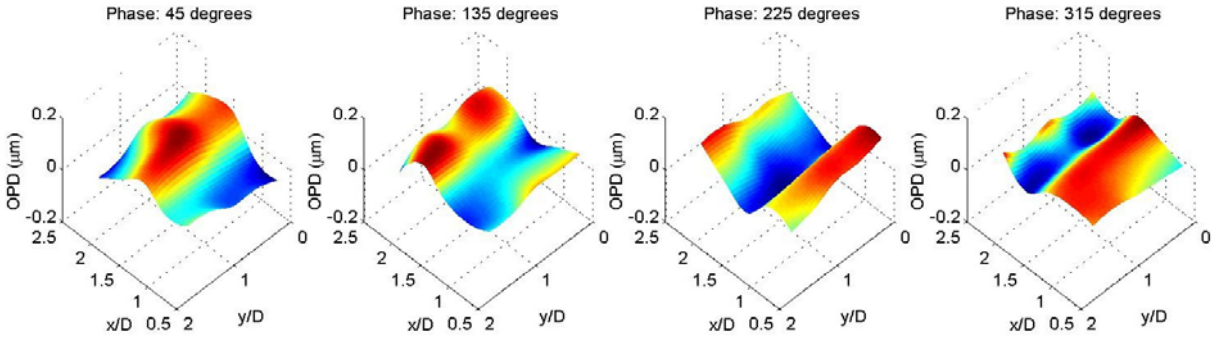

Figure 13. Phase-averaged wavefronts obtained with the high-bandwidth wavefront sensor.

high-bandwidth wavefront sensor has only a modest spatial resolution of 4 X 4 apertures, it captures all essential features of the flow-induced aberrations, including the development of the roll-up structure by x/D = 1, it's spanwise-uniform nature and even evidences of pairing events around x/D = 2.

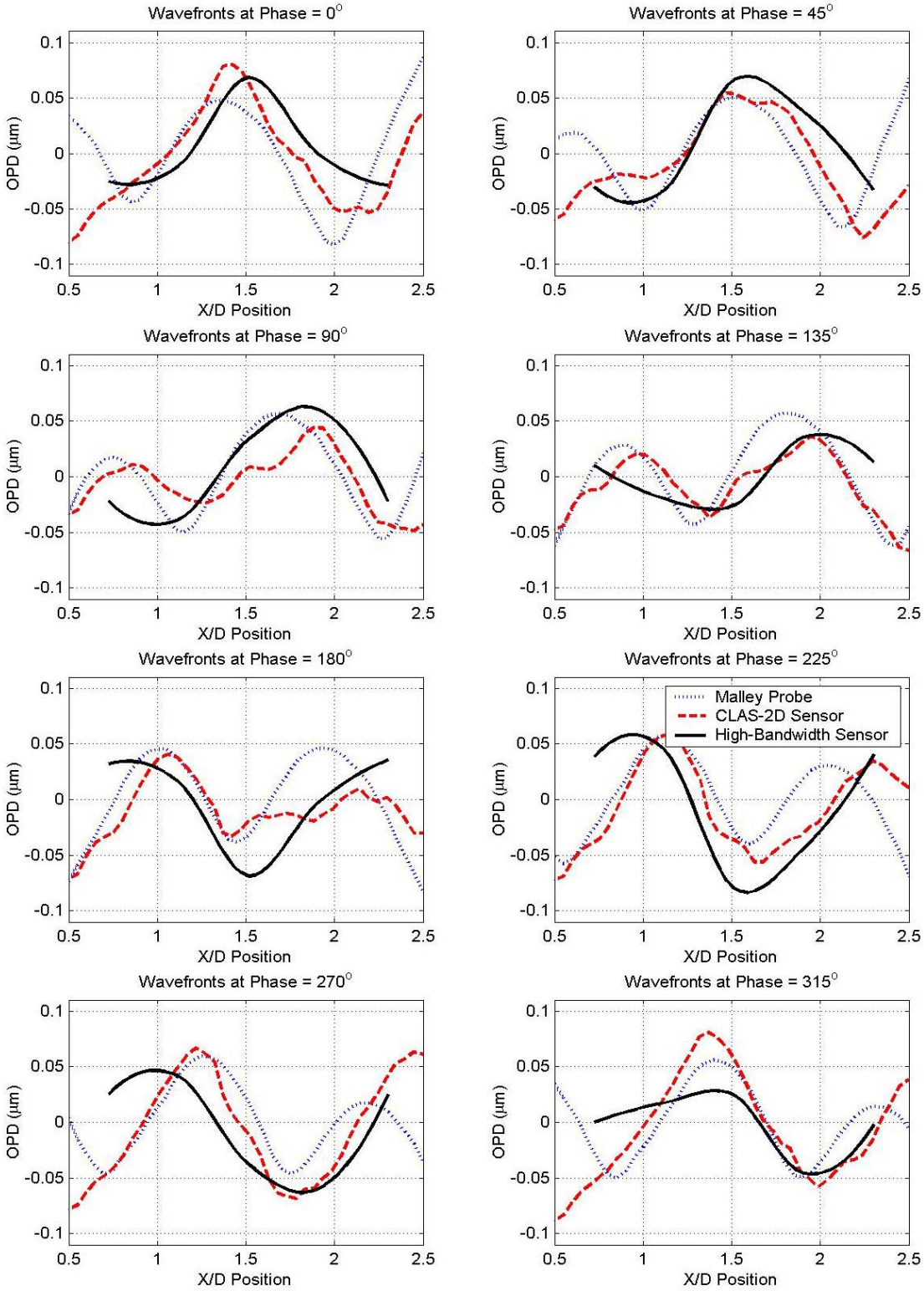

Figure 14. Phase-averaged wavefronts obtained with the high-bandwidth wavefront sensor at various phase angles.

A comparison of all three wavefront-sensing techniques over an aperture from *X/D* = 0.5 to *X/D* = 2.5 is given in Figure 14. Both the CLAS-2D and the high-bandwidth wavefront sensors data were averaged in the spanwise direction to get one-dimensional slices of wavefronts along the streamwise direction for a fair comparison with the Malley probe data. Figure 14 not only shows that all wavefront sensors' peak-to-peak amplitude measurements are of the same order, but many essential flow features are captures by all sensors. The CLAS-2D wavefront sensor gives a good spatial resolution of the underlying flow structure, but it is clear that four sub-apertures in the streamwise direction used in the high-bandwidth wavefront sensor are sufficient to resolve the main roll-up structure and correctly measure its position and amplitude. It is important to note that the optical signal has a modest peak-to-peak amplitude of no more than 0.25 microns, yet all sensors were able to correctly resolve optical wavefronts.

It is important to note that the Malley Probe extends the wavefront information upstream and downstream by presuming that the frozen-flow hypothesis is strictly true. It is clear in the Figure 14 comparison that there are discrepancies the full-aperture direct measurement made by the CLAS-2D wavefront sensor and the Malley probe data, primarily due to the breakdown in the frozen-flow hypothesis at x/D = 0.5..1, were the roll-up structure is yet to be developed. The extrapolated Malley wavefronts do a decent job predicting the wavefront in the downstream direction of the beams' locations, but grossly over predict the wavefronts upstream of the probe beams. This can be attributed to the fact that the flow structures are evolving rapidly in those regions; initial vortex roll-up is occurring in the upstream region while vortex pairing is occurring in the downstream region. Aperture size effects and extensive testing of the Malley probe is described in Duffin et. al. (2004), where it was concluded that the Malley probe and the two-dimensional wavefronts provide virtually the same results for smaller apertures where the frozen field assumption holds.

4.4 Effect of removing phase-averaged structure from instantaneous wavefronts.

If the flow is locked into a periodic pattern it is possible to use the phase-locked averaged time series of high-frequency wavefronts, as in Figure 13, to remove most of the optical aberrations using a feed-forward "adaptive-optics" scheme. In such a scheme, one might imagine having a high-frequency bandwidth deformable mirror being driven at a pre-defined time-changing

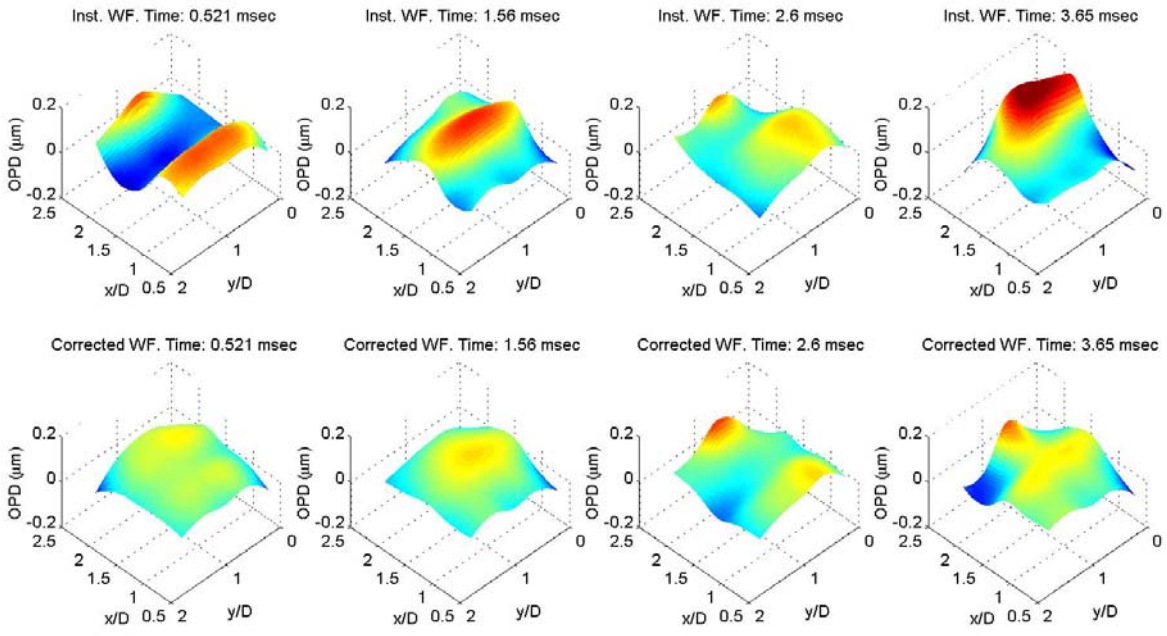

Figure 15. Instantaneous (upper row) and corrected (bottom row) wavefronts.

aberration pattern. Using highly temporally resolved wavefronts obtained with the high-bandwidth wavefront sensor allows us to investigate the effects of such an adaptive-optics approach. Let us assume we had programmed a deformable mirror to remove a phase-averaged wavefronts locked with the 240 Hz forcing frequency as given in Figure 13. Then, using a mirror update rate of 6 kHz would give 24 mirror updates per forcing period. Now we can check a residual wavefronts to estimate an effectiveness of such control strategy. Figure 15 present several instantaneous wavefronts (upper row) and the same wavefronts with the phase-average aberrations removed (lower row). Corrected wavefronts exhibit smaller amplitudes and most of the optical aberrations related to the roll-up structure passing across the aperture are effectively removed from the instantaneous wavefronts simulating what would be done by a the deformable mirror.

Usually one is interested in an amount of intensity on a target, described by a Strehl ratio *St*. The higher the Strehl ratio, the higher the intensity on the target. Since the Strehl ratio depends on the laser wavelength, we calculated the instantaneous Strehl ratio for the laser wavelength of 0.5 microns, with and without the "adaptive-optics" corrections, presented in Figure 15. The results are shown in Figure 16. The dotted line represents the case with no correction applied. Deep drops in the Strehl ratio are apparent when the roll-up structure passes across the beam aperture, when the Strehl ratio drops down to a value of 0.4 to 0.5. The average Strehl ratio is about 0.7 for the forced heated jet without correction, meaning an on-average loss of 30% of the intensity on the target. But when the adaptive optics corrections are applied, the solid line in Figure 15 shows that the Strehl ratio is dramatically improved. With the degrading aero-optical effects of the roll-up structure compensated the average Strehl ratio jumps to 0.9.

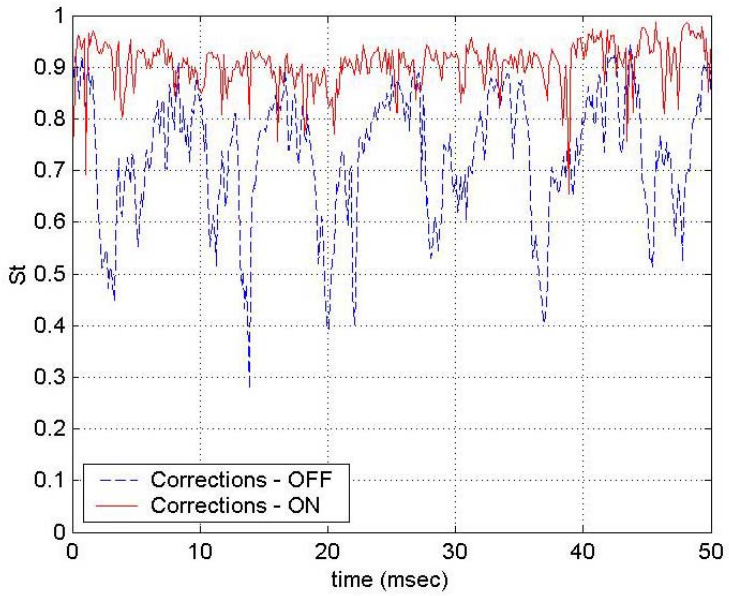

Figure 16. Strehl ratio with and without the adaptive optics corrections at the wavelength of 0.5 microns.

5. Conclusions.

Two analog wavefront measuring devices were developed and tested at the University of Notre Dame. The analog nature of these sensors allows for high, on the order of tens and hundreds of kilohertz' sampling rates and long time series of wavefronts, which is crucial for investigating and correcting aero-optical effects.

The Malley probe measures one-dimensional slices of optical wavefronts in the streamwise direction with both high spatial and temporal resolution. The two probe-beam approach enables

the measurement of the convective speeds of optically-active structures in turbulent flows and also provides a basis for removing vibration-related and other non-physical contaminations always present in a tunnel environment. The simple set-up, compactness and easy-to-adapt configuration make this instrument a valuable research tool for aero-optical measurements.

The high-bandwidth two-dimensional wavefront sensor in its simplest configuration measures wavefronts over 4 X 4 sub-apertures with temporal sampling rates up to 125 kHz. The sensor modular design allows to gang two, three or four of them together to achieve higher spatial resolution of 4 X 8 or 8 X 8 sub-apertures.

Both devices were tested on an acoustically-forced heat jet facility and compared to a commercially available two-dimensional wavefront sensor with a 33 X 44 sub-aperture spatial resolution. It was shown that both of the high-bandwidth sensors correctly resolved all the essential features of the roll-up structure evolution, including the convective nature and amplitude of the optical aberrations. Phase-averaged wavefronts were collected and an open-loop adaptive optics approach was shown to be highly effective in reducing degrading aero-optical effects in the periodic forced turbulent flow.

6. Acknowledgements.

This effort was sponsored in part by the Air Force Office of Scientific Research, Air Force Material Command, USAF, under Grant Number F49620-03-1-0019. The U.S. Government is authorized to reproduce and distribute reprints for governmental purposes notwithstanding any copyright notation thereon. The effort was also sponsored in part by ITAC, Ltd. and Oceanit.

List of Movies

Movie 1: Phase–averaged wavefronts obtained with the high-bandwidth wavefront sensor (687 kB)

References

Cicchiello, J. and Jumper, E., "Far-Filed Optical Degradation due to to Near-Field Transmission Through a Turbulent Heated Jet", Applied Optics, Vol. 36, No. 25, 1997, pp. 6441-6452.

Duffin, D., Gordeyev, S. and Jumper, E., "Comparison of Wavefront Measurement Techniques on a Two-Dimensional Heated Jet", AIAA Paper 2004-2406, Portland, June 2004.

Duffin, D. A., Gordeyev, S., and Jumper, E. J., "Visualizing Index-of-Refraction Variations in Optically Active Flow Fields," 11th International Symposium of Flow Visualization Conference, Paper# 075, Notre Dame, IN, 2004.

Geary, J. M., "Introduction to Wavefront Sensors," Tutorial texts in Optical Engineering, Vol. TT18, Bellingham, WA, SPIE Optical Engineering Press, 1995.

Gilbert, K. J. and Otten L. J. (eds), Aero-Optical Phenomena, Progress in Astronautics and Aeronautics, Vol. 80, AIAA, New York, 1982.

Gordeyev, S., Jumper, E. J., Ng, T., and Cain, A., "Aero-Optical Characteristics of Compressible, Sub-sonic Turbulent Boundary Layers," AIAA Paper 2003-3606, Orlando, June 2003.

Jumper, E.J., and E.J. Fitzgerald, "Recent Advances in Aero-Optics", Progress in Aerospace Sciences, Vol. 37, 2001, pp.299-339.

Hugo, R. J., "Quantifying the Spatio-Temporal Effects of Optically-Active Turbulent Flowfields on a Coherent Optical Wave," Ph.D. Dissertation, Department of Aerospace and Mechanical Engineering, University of Notre Dame, Notre Dame, IN, 1995.

Hugo, R. J., and Jumper, E. J., "Implications of the Homogeneous Turbulence Assumption on the Aero-Optic Linking Equation," Optical Techniques in Fluid, Thermal, and Combustion Flow, Vol. 2546, edited by S.S. Cha and J.D Trollinger, SPIE—International Society of Optical Engineering, Bellingham, Washington, USA, 1995a, pp. 189-200.

Hugo, R. J., and Jumper, E. J., "Constant Current Anemometry and its impact on Aero-Optical Measurements," AIAA Paper 95-1986, Jun. 1995b.

Hugo, R. J., and Jumper, E. J., "Quantification of Aero-Optical Phase Distortion Using the

Small-Aperture Beam Technique," AIAA Journal, Vol. 33, No. 11, 1995c, pp. 2151-2157.
Hugo, R. J., and Jumper, E. J., "Experimental Measurement of a Time-Varying Optical Path Difference by the Small-Aperture Beam Technique," Applied Optics, Vol. 35, No. 22, Aug. 1996, pp. 4436.
Malley, M., Sutton, G. W., and Kincheloe, N., "Beam-Jitter Measurements of Turbulent Aero-Optical Path Differences," Applied Optics, Vol. 31, 1992, pp. 4440-4443.
Southwell, W. H., "Wave-front Estimation from Wave-front Slope Measurements", J. Opt. Soc. Am., Vol. 70, N0, 8, 1980, pp. 998-1006.